

## Feature of catalysis on bimetallic alloys Zr with V, Mo, and Fe in the reaction of methanol oxidation

Arif EFENDI<sup>1</sup>, Lala MAGERRAMOVA<sup>1,2</sup>, Adila ALIYEVA<sup>1</sup>, Lyudmila KOJA-ROVA<sup>1</sup>, Elmira BABAYEV<sup>1\*</sup>

<sup>1</sup>Ecological Catalysis Department, Institute of Catalysis and Inorganic Chemistry, Azer-baijan National Academy of Sciences, Baku, Azerbaijan

<sup>2</sup>Department of Physical and Colloidal Chemistry, Faculty of Chemistry, Baku State Uni-versity, Baku, Azerbaijan

Received: 06.10.2020 • Accepted/Published Online: 08.04.2021 • Final Version: 27.08.2021

**Abstract:** Catalytic behaviors of bimetallic catalysts-alloys of zirconium with vanadium, molybdenum, and iron was investigated in the oxidative dehydrogenation of methanol. The conditions for the formation of the catalyst's active surface were revealed. The conversion of methanol into formaldehyde, dimethyl ether, and dimethoxymethane on bimetallic catalysts was studied. The characterization of catalysts was performed by XRD, XPS, and SEM. It was shown that the activity of samples increases after O<sub>2</sub> + H<sub>2</sub> treatment and was associated with segregation of the active components of alloys (V, Mo) on the surface of catalysts and realization of their optimal oxidation state under catalysis conditions.

**Key words:** Bimetallic catalysts, methanol oxidation, redox treatment, formaldehyde, dimethyl ether, dimethoxymethane

### 1. Introduction

Bimetallic catalysts and their industrial application on worldwide scale in petroleum reforming processes have played an important role in production of valuable hydrocarbons (lead-free gasoline, safe for environment) [1,2]. Bimetallic systems, unlike monometallic catalysts, are more active and selective, and require further investigations. Combinations of adjacent atoms in volume, the influence of the so-called "electronic factor", preactivation conditions are the causes of increased interest.

Selective catalysts of methanol oxidation are mainly metals, metal oxides, heteropoly acids and zeolites. Methanol is a cheap and accessible raw material for the production of formaldehyde, dimethyl ether, and dimethoxymethane.

Formaldehyde (FA) has been used as a synthesis baseline for many chemical compounds, including phenol-formaldehyde, urea formaldehyde, and melamine resin. It is produced by catalytic partial oxidation of methanol over Cu-oxide catalyst and polycrystalline Ag-catalyst [3,4]. The other route involves the oxidation of methanol over catalyst of Mo-Fe oxides [5].

Dimethyl ether (DME) has been used as an aerosol propellant, a clean alternative fuel for diesel engines, which results in lower exhaust emissions. DME can be achieved directly from CH<sub>3</sub>OH over different catalysts, such as  $\gamma$ -Al<sub>2</sub>O<sub>3</sub>; HZSM-5; Cu/ZnO/Al<sub>2</sub>O<sub>3</sub> [6,7].

Dimethoxymethane (DMM) has been used as a solvent in the pharmaceutical and perfumery industries due for its low toxicity. It is also used as a diesel fuel additive, has a high cetane number (> 80). Catalysts such as rhenium oxides [8], MoOx/TiO<sub>2</sub> [9], modified with VO<sub>x</sub>/TS-1 [10], and V-complex oxides [11,12] showed a good performance in the selective oxidation of methanol. Vanadium oxides, as highly efficiently catalysts, are widely applied in various catalytic reactions, such as the dehydrogenation hydrocarbons [13]. All these catalysts are complex systems, the study of activities of which is difficult due to influence of numerous factors. However, in bimetallic catalyst systems, introduction of the second component creates the possibility of varying catalytic properties in a wide range [14].

Vanadium oxide-based catalysts are well known and extensively employed in industry for the gas phase heterogeneous oxidation of hydrocarbons and for the oxidative dehydrogenation of C<sub>2</sub>-C<sub>4</sub> alkanes and alcohols [15]. During the oxidation of methanol, as it was described in the previous studies [15,16], the catalytic activity of supported vanadium catalysts decreased in the following trend: VO<sub>x</sub>/ZrO<sub>2</sub>>VO<sub>x</sub>/(Al,Zr-oxides) > VO<sub>x</sub>/Al<sub>2</sub>O<sub>3</sub> and was dependent on the nature of the

\* Correspondence: [elmir.magsadoglu@gmail.com](mailto:elmir.magsadoglu@gmail.com)

support. Formaldehyde was the main reaction product on catalysts supported on Zr-containing oxides (which can be related to a low amount of acid sites). However, dimethyl ether was mainly observed on alumina-supported vanadium oxide catalysts (which is linked to the presence of acidic sites on the surface of the catalyst, as determined by TPD-NH<sub>3</sub>). Further studies showed [17–23] that following factors had a great impact on the catalytic behavior of vanadium-supported catalysts: (i) the nature of V<sup>n+</sup>–O species, i.e., coordination, aggregation, and oxidation state of V-species; (ii) redox properties of the catalysts, i.e., the V<sup>5+</sup>/V<sup>4+</sup> ratio in reaction, (iii) acid–base character of the catalysts (as well as the support), that determines the selectivity of reaction products.

It is well-known that the support of ZrO<sub>2</sub> has bifunctional redox properties of both an acid and a base, as well as possessing a great thermal stability. By modifying the aluminum oxide support by adding ZrO<sub>2</sub>, it was possible to obtain a more efficient catalyst for the dehydrogenation of ethane and methanol [15,17]. The study showed that both ZrO<sub>2</sub> [18], and Al<sub>2</sub>O<sub>3</sub>-ZrO<sub>2</sub> [19,20] are appropriate supports for the synthesis of highly dispersed VOx-species [20,24,25]. As shown by XRD patterns, supported vanadium oxide VOx can exist on these supports in the form of isolated tetrahedral monovanadates, one- or two-dimensional polyvanadate domains, or bulk V<sub>2</sub>O<sub>5</sub> crystallites [21].

Oxygen particles that bind surface vanadium oxide particles to the support can play an important role in catalyst activity. Thus, the VO↔ bond on the support mainly determines its catalytic characteristics. In the vanadium oxide catalysts support on pure ZrO<sub>2</sub>, the presence of both monoclinic and tetragonal crystallites of ZrO<sub>2</sub> and V<sub>2</sub>O<sub>5</sub> (in the sample with the highest V load) was found. Moreover, the presence of mixed oxides Zr-V, such as ZrV<sub>2</sub>O<sub>7</sub>, cannot be excluded [15,22].

Quantum-chemical evaluations of the V<sub>2</sub>O<sub>5</sub> structure revealed two types of crystal planes [23]. On the (100) and (001) planes, the cleavage leaves coordination unsaturated vanadium and oxygen ions, which develop Bronsted acid-base interactions with the reacting molecules. The equilibration of gas phase oxygen with vanadium oxides leads to the formation of an internal defect structure of V<sub>2</sub>O<sub>5</sub>, consisting of oxygen vacancies. In the previous studies [24–28] the unique physical and chemical characteristics of supported vanadium catalysts in comparison with other catalysts supported by metal oxides for hydrocarbon oxidation reactions were discussed, covering the required number of surface vanadium centers, the effect of metal oxide additives, the effect of acidic and basic centers on the surface, the effect of preparation methods and the effect of a specific phase of the oxide substrate.

The acid-base character of the metal oxide support affects the dispersion of vanadium on the surface of the support, as well as the nature of the vanadium species. The reducibility and structure of surface vanadium oxide particles and the acid-base character of catalysts, in addition to their catalytic properties in the oxidative dehydrogenation of alkanes, strongly depend on the metal oxide used as a support and the vanadium content of the V<sup>5+</sup> tetrahedral species [19].

Molybdenum catalysts are less active than vanadium ones, however, catalytic properties increase on zirconium oxide ZrO<sub>2</sub>. The impact of the support structure, as well as acid sites and dispersion were studied [29]. In order to enhance the activity of MoO<sub>3</sub>/ZrO<sub>2</sub>, preliminary treatment with hydrogen, the introduction of vanadium as a second component was proposed. The activity of the Mo<sup>5+</sup> ion in catalytic processes has been confirmed in a number of studies. Thus, in a study by C. Ranga et al. [30] an evaluation of the surface composition and state of Mo surface particles was carried out on samples of MoO<sub>3</sub>/ZrO<sub>2</sub> catalysts, fresh and reduced with H<sub>2</sub>/CH<sub>4</sub> (XPS). The fresh sample contained only Mo<sup>6+</sup> particles, and moderate reduction of the MoO<sub>3</sub> sample at T 623 K resulted in the presence of Mo<sup>5+</sup> particles along with Mo<sup>6+</sup>, as well as Mo<sup>4+</sup>. The presence of Mo<sup>5+</sup> particles in reduced samples, according to the authors, indicated the creation of active defects in the structure of the starting oxide, which led to an increasing activity. It was also reported that Mo<sup>5+</sup> particles appeared as a result of the reduction of MoO<sub>3</sub> to MoO<sub>3-x</sub>. Interesting studies of the selective oxidation of methanol in DMM were carried out on the V<sub>2</sub>O<sub>5</sub>-MoO<sub>3</sub>/γ-Al<sub>2</sub>O<sub>3</sub> catalysts by Yali Meng et al. [31]. These catalysts exhibit better DMM yield characteristics than the corresponding samples containing only V and Mo particles, even at relatively low temperatures. By adjusting the V content, catalysts were investigated and explained by the synergistic effect of mixed oxides of V and Mo that are present on the catalyst surface. The redox cycle of V-O-Mo oxides can be completed through the transfer of electrons between lattice oxygen and metal cations. V species exhibit superior performance in adsorption and activation of oxygen gas, as well as an increased ability to reduce lattice oxygen and suppress Mo particle aggregation. 14V<sub>2</sub>O<sub>5</sub>-14MoO<sub>3</sub>/Al<sub>2</sub>O<sub>3</sub> catalyst with an optimized number of redox and acid sites was obtained, which have demonstrated a methanol conversion of 54% with a DMM selectivity of 92% at 393 K.

All considered vanadium and molybdenum catalysts belong to supported oxides, with different methods of preparation. The correlation of their activity with the type of support, acidity, structure, number of redox centers was examined. However, research studies on alloys has not been conducted. We tried to carry out such evaluation of oxidative dehydrogenation of methanol, which appeared to be overly sensitive to the effects of various factors. Alloys can be considered the models, on which conditions, affecting the formation of the active surface can be studied [32,33].

## 2. Experimental

### 2.1. Chemicals and reagents

All chemicals and reagents were of analytical grade and used without any further treatment. The following materials were used to prepare alloy samples: molybdenum (powder, TC 48-19-316-80, purity ~99.5%; melting temperature 2.89 K), Vanadium (ingots, TC48-4-272-73, purity ~99.4%; melting temperature 2.160 K), Zirconium (ingots, manufacturer YWBL-WH, purity ~99.4%; melting temperature 2.128 K), iron (powder, OCHV. Ru., purity~99.8%; melting temperature 1.812 K), absolute methanol (99.9%; AzMeCo).

### 2.2. Catalyst preparation

Initial samples of Zr alloys with V, Mo, and Fe of various compositions were prepared by fusing metal weighed portions in an arc furnace based on the ratio of atomic weights, for example: intermetallic compound  $ZrMo_2$ ;  $A_r(Zr) = 91.224$ ;  $A_r(Mo) = 95.94$ .

$$M_r(ZrMo_2) = 91.224 + 2 \times 95.94 = 91.224 + 191.88 = 283.104.$$

$$\text{Molybdenum content} \quad 191.88: 283.1 = 67.8 \text{ wt.\% Mo.}$$

$$\text{Zirconium content} \quad 91.224: 283.1 = 32.2 \text{ wt.\% Zr.}$$

To obtain 20 g of  $ZrMo_2$  alloy:  $20.0 \times 0.678 = 13.6$  g Mo and 6.4 g Zr are needed.

After melting,  $ZrMo_2$  ingot weighing – 17.6 g;  $\Delta = -2.4$  g was obtained.

Following samples of catalysts were obtained and showed in Table 1:

$$ZrV_{0.3}; Zr_{0.6}; ZrV; ZrMo_{0.5}; ZrMo; ZrMo_2, VFe_{0.2}; VFe_{0.3}; VFe_{0.6}.$$

The metal weighed portions were preliminarily pressed, then fused in an arc furnace in an atmosphere of high purity helium. To obtain homogeneous uniform alloys the ingots were re-melted 2–3 times until uniform homogeneity was obtained. Samples of catalysts, then grounded to a particle size of 0.06–0.10 mesh, were mixed with crushed glass, quartz, and then placed into a tubular quartz reactor. The preliminary oxidative treatment of the catalysts was carried out in the air stream at T 873 K 3–4 h, and reducing treatment was carried out in the hydrogen stream at T 873 K for 1 h.

### 2.3. Characterization

Changes in the activity of catalysts are associated with phase changes in the surface layer, thus, X-ray diffraction analysis (XRD) of catalysts were carried out before and after  $O_2 + H_2$ -treatment on Rigaku Mini Flex 600 X-ray diffractometer ( $k\lambda$  1.54060 Å) using Ni- filtered  $CuK\alpha$  radiation, powder diffractometer Bruker “D2 Phaser” and DRON-2 with  $CuK\alpha$  radiation.

Changes were observed not only in the composition of the surface layer, but also in the valence state of the active components of alloys (V, Mo), as indicated by the results of X-ray photoelectron spectroscopy (XPS), which was carried out on VIEE-15 and ADES-400 spectrometer. The specific surface area of the catalyst samples was determined using Thermo Scientific SURFER. The scanning electron microscope (SEM) HITACHI S-3400N was used for the observation of specimen surfaces.

### 2.4. Experimental part

The examination of the catalytic activity of alloy samples was carried out in a quartz reactor at pulsed and flow modes (weighed number of catalysts for a pulse unit - 0.2 g; for a flow-through unit - 0.3 g). On a pulse installation carrier gas,

**Table 1.** Compositions of the obtained catalysts.

No	Catalyst	Sample composition, (% wt).	Amount, g	Weight, g
1	$M_r(ZrMo_2) = 283.10$	$ZrMo_2$ (67.8 Mo)	6.4 Zr + 13.6 Mo	20.0 $ZrMo_2$
2	$M_r(ZrMo) = 187.16$	ZrMo (51.3 Mo)	7.3 Zr + 7.7 Mo	15.0 ZrMo
3	$M_r(ZrMo_{0.5}) = 139.22$	$ZrMo_{0.5}$ (34.48 Mo)	9.82 Zr + 5.18 Mo	15.0 $ZrMo_{0.5}$
4	$M_r(ZrV) = 142.16$	ZrV (35.83 V)	12.84 Zr + 7.16 V	20.0 ZrV
5	$M_r(Zr_{0.6}) = 121.79$	$ZrV_{0.6}$ (25.09 V)	14.98 Zr + 5.02 V	20.0 $ZrV_{0.6}$
6	$M_r(Zr_{0.3}) = 105.6$	$ZrV_{0.3}$ (14.35 V)	17.13 Zr + 2.87 V	20.0 $ZrV_{0.3}$
7	$M_r(VFe_{0.6}) = 84.45$	$VFe_{0.6}$ (39.68 Fe)	12.06 V + 7.94 Fe	20.0 $VFe_{0.6}$
8	$M_r(VFe_{0.3}) = 67.70$	$VFe_{0.3}$ (24.76 Fe)	14.06 V + 4.94 Fe	20.0 $VFe_{0.3}$
9	$M_r(VFe_{0.2}) = 62.11$	$VFe_{0.2}$ (17.98 Fe)	16.4 V + 3.6 Fe	20.0 $VFe_{0.2}$

helium from the chromatograph system entered a quartz reactor, into which, at T 473–673 K, samples (methanol) are injected using a micro syringe. The experiment was carried out both with an air supply (through a dispenser) and without air. After reactor, the products, together with helium carrier-gas, enter to the separation column of the chromatograph (GC); filled with Porapak-Q (3m), then flow into the thermal conductivity detector and further to TSVET-500 chromatograph recorder. The column temperature was maintained within the range of 413–418 K.

On a pulsed installation, the reactor was placed in an electrically heated furnace. The reaction temperature has been controlled by a thermocouple (TXK), placed inside the catalytic reactor at the level of the catalyst bed. Additional conditions of the experiment will be explained in section 3.2.

On a flow-through unit, alcohol vapors, taken up by nitrogen, passed through the distillation plates of the saturator, then entered the mixer, where purified, dried oxygen was supplied. The mixer was placed in the thermostat, where a constant temperature of 423 K was maintained. The gas mixture was fed into a quartz reactor heated in a thermocouple controlled furnace. The off-gas measurement (and contact time) was carried out using a GSB-400 drum gas meter. The time to reach the stationary mode was determined according to the constant composition of the outgoing reaction mixture; average time was ~ 20–30 min. When the stationary regime was reached, the gas flow was switched on a six-way valve at the outlet of the reactor, staying at position 2 (sampling). At the same time, the value of the reactor temperature, flow rate, O<sub>2</sub>/N<sub>2</sub> ratio, alcohol flow temperature at the outlet from the saturator, partial pressures P<sub>sp</sub>; P<sub>o<sub>2</sub></sub>; alcohol/O<sub>2</sub> ratio were measured and noted.

Samples of alloys did not show catalytic activity in the oxidation of methanol until T 673--773 K. However, after O<sub>2</sub>-treatment with air at T 873 K for 3 h an increase of activity was observed. After reduction treatment in a stream of hydrogen at T 873 K for 1 h, the activity of the catalyst increased sharply (a scheme of a flow-through installation is given in the appendix in Supplemental Figure 1S).

### 3. Results and discussion

#### 3.1. Catalysts characterization

The initial samples of alloys did not show catalytic activity in the oxidation of methanol until T 773 K, however, at the temperature above T 773 K the formation of products of deep oxidation and decomposition was observed. Treatment in vacuum, flow of helium, and hydrogen did not lead to any change in the activity. Only after oxidative treatment with air at T 873 K for 1 h, the catalysts began to show activity, and after 3-h air treatment, the activity of the samples increased and stabilized. It is well known that when an alloy encounters any adsorbate, its surface becomes enriched with a metal that forms a stronger bond with this adsorbate. In terms of oxygen, zirconium possesses a high affinity for it, based on thermodynamic calculations ( $\Delta G_{\text{ZrO}_2} = -1039$  kJ/mol;  $\Delta G_{\text{V}_2\text{O}_4} = -334$  kJ/mol;  $\Delta G_{\text{V}_2\text{O}_5} = -365.6$  kJ/mol), where  $\Delta G$  — Gibbs function. X-ray diffraction analysis (XRD) of the samples showed that on the catalyst surface, zirconium is mainly present in the oxidized phase (see Figure 1a).

The X-ray diffraction pattern of the initial ZrV<sub>0.3</sub> sample, showed peaks at  $2\theta = 32.0^\circ; 35.7^\circ; 51.59^\circ; 62.3^\circ; 67.5^\circ$ , which could be associated with the presence of both monoclinic and tetragonal structures of ZrO<sub>2</sub> (JCPDS: 37-1484, 17-923). Peaks at  $2\theta = 32.0; 35.8; 40.1; 54.9$  were associated with the presence of metallic zirconium (JCPDS: 5-665). Thus, following products were found on the surface of the initial sample: mainly metallic Zr, m-ZrO<sub>2</sub>; t-ZrO<sub>2</sub>. Vanadium and vanadium oxides were absent. After O<sub>2</sub>-treatment with air (T 873 K, 3 h), the activity of the catalyst increases, which is associated with phase changes in the surface layer (Figure 1b; Supplemental Tables 1 and 2).

The peaks that appeared on the diffractogram are associated with the presence of mixed oxides - orthorhombic m-V<sub>2</sub>O<sub>5</sub> on the catalyst surface (at  $2\theta = 20.3; 26.2; 31.2; 34.3; 47.3; 50.5$ ; JCPDS: 41-1426), tetragonal t-V<sub>2</sub>O<sub>5</sub> (at  $2\theta = 18.6; 23.6; 30.2; 35.5; 44.5; 50.7; 53.5; 57.4; 61.0$ ; JCPDS: 79-1976), V<sub>2</sub>O<sub>3</sub> (at  $2\theta = 23.6; 32.7; 37.6; 41.8; 53.9$  JCPDS: 34-0187). The  $2\theta$  values for VO<sub>2</sub>, V<sub>4</sub>O<sub>9</sub> oxides are remarkably close, that lead to the failure to identify them (JCPDS: 81-2392; 43-1051).

Although V<sub>2</sub>O<sub>5</sub> and V<sub>2</sub>O<sub>3</sub> oxides were present on the surface of the ZrV<sub>0.3</sub> catalyst after O<sub>2</sub>-treatment, the activity of the sample in the oxidation of methanol increased insignificantly (the conversion of CH<sub>3</sub>OH at T 473K was 9.6%, and at T 573K- 46.2%). Only after H<sub>2</sub>-treatment, the activity of the catalysts increases drastically, which can be seen from Figures 2–4 for Zr-V, Zr-Mo and V-Fe alloys.

The study of methanol conversion, presented in these figures, was performed in a pulsed mode. Carrier gas, helium, from the chromatograph system entered the reactor, and then moved to separating column and to the thermal conductivity detector. Methanol was introduced with a microsyringe (1–2  $\mu\text{L}$ ) at a temperature range 473–573 K, in the presence of oxygen and without it. The experiments were carried out for a long time (10–20 h) in order to check the activity of the catalyst samples and to select the most active ones. The reaction products contained FA, DME, DMM, and MF. The data of these experiments were confirmed later when carrying out the reaction in a flow-through unit explained in section 3.2.

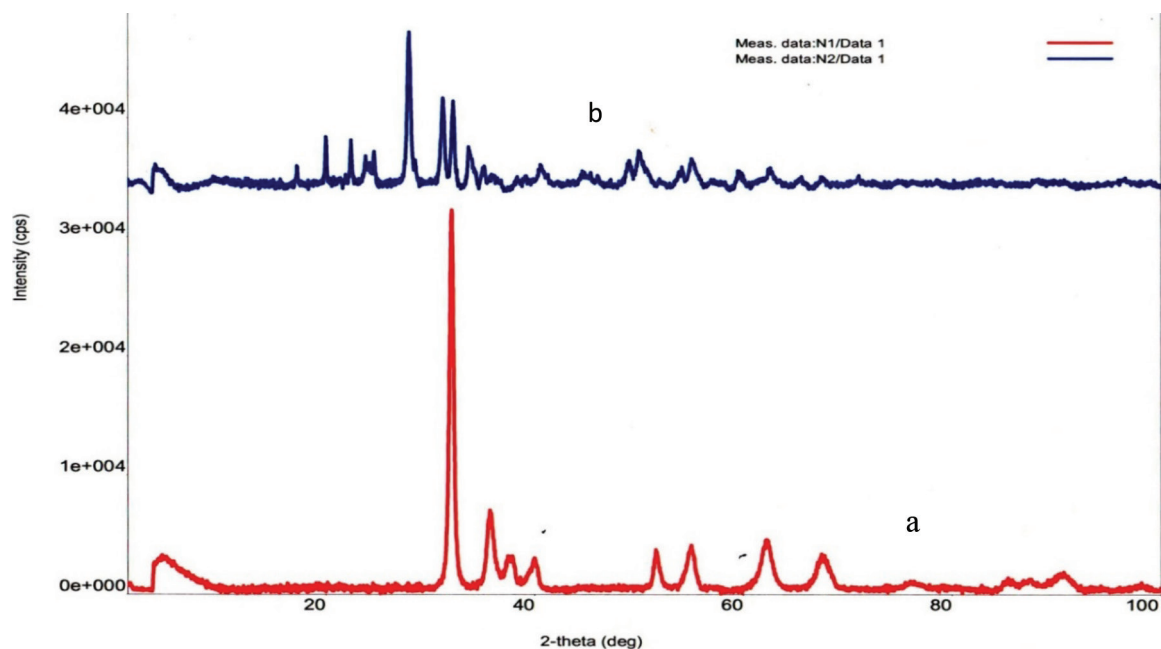


Figure 1. XRD patterns of catalyst based on an alloy  $ZrV_{0.3}$ : a) initial  $ZrV_{0.3}$ ; b) after  $O_2$ -treatment, T 873 K, 3 h.

Table 2. X-ray photoelectron spectroscopy of alloy  $ZrMo_2$  after treatments.

№	Terms of processing	Mo content in oxidation state, %			Mo/Zr	$\frac{I_{0.1S}}{I_{Zr\ 3d} + I_{Mo\ 3d}}$
		VI	IV	0		
1	Initial $ZrMo_2$	49	21	30	1.1	0.6
2	Vacuum, T 673 K	9	5	86	1.1	0.3
3	Air, T 873 K, 3 h	100	0	0	1.4	0.6
4	Hydrogen, 873 K, 1 h	22	-	78	1.4	0.6
5	Air, T 873 K, 3 h + Hydrogen, T 873 K, 1 h + Catalysis	65	35	-	1.4	0.6

If vanadium was absent on the surface of the initial  $ZrV_{0.3}$  sample, after  $O_2$ -treatment it emerged to the surface, enriched of the surface layer with vanadium (segregation) and later oxidized. The V/Zr ratio in the surface layer increased.  $ZrO_2$  oxide remained at the bottom of the catalyst as a support. Deep phase changes in the surface layer were also observed for the  $ZrMo_2$  catalyst after  $O_2$ -treatment (T873 K, 3 h), following by  $H_2$ -treatment (T873 K, 1 h), as it is described at Figures 5.

Mainly the phase of zirconium molybdate  $Zr(MoO_4)_2$  is formed on the surface of the  $ZrMo_2$  catalyst after  $O_2$ -treatment. The experimental data and the data of the reference diffraction patterns coincide. In addition, there were slightly shifted peaks corresponding to  $MoO_3$ ; no noticeable increase in the activity of the catalyst was observed. However, after  $H_2$ -treatment (T 873 K, 1 h), the activity of the catalyst increased sharply, and at a reaction temperature of 473 K the methanol conversion was 56.5% - Figure 3. The increase in activity was associated with phase changes on the sample surface (Supplementary Tables 3 and 4).

After  $O_2$ -treatment it was possible to identify the  $Zr(MoO_4)_2$  phase only on the  $ZrMo_2$  intermetallic compound. However, after  $H_2$ -processing, the largest peaks at  $2\theta = 15.646; 21.034$  ( $d = 5.642\text{\AA}, 4, 231\text{\AA}$ ) did not correspond to any of the oxide compounds of molybdenum. Peaks at  $2\theta = 22.6; 24.7; 26.2$  were close to nonstoichiometric  $i-Mo_4O_{11}$  oxides ( $d = 3.93\text{\AA}, 3.60\text{\AA}; 3.41\text{\AA}$ ; card 13-142), with  $2\theta = 24.84; 26.41; 27.25$  - corresponding to  $Mo_9O_{26}$  ( $d = 4.00\text{\AA}; 3.75\text{\AA}; 3.48\text{\AA}$ ; card 12-753). Formation of other nonstoichiometric  $MoO_x$  oxides are possible. Peaks observed at  $2\theta = 56.46; 68.65; 76.9$ ; refer to recovered, partially metallic molybdenum (JCPDS: 01-1208). According to the diffraction pattern, the surface composition is characterized by  $H_6Mo_2O_{11}Zr$  formula.

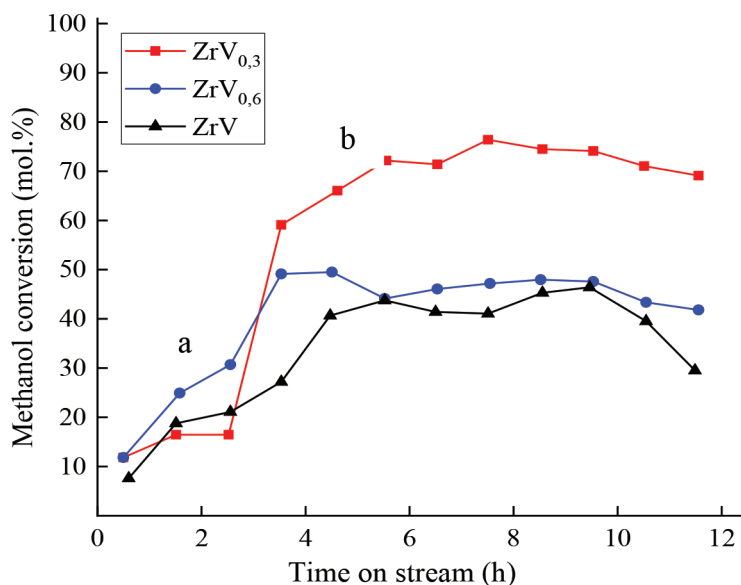


**Figure 2.** Variation of methanol conversion on catalysts Zr-V: a) after O<sub>2</sub>-treatment; b) after H<sub>2</sub>-treatment, reaction temperature 473 K.

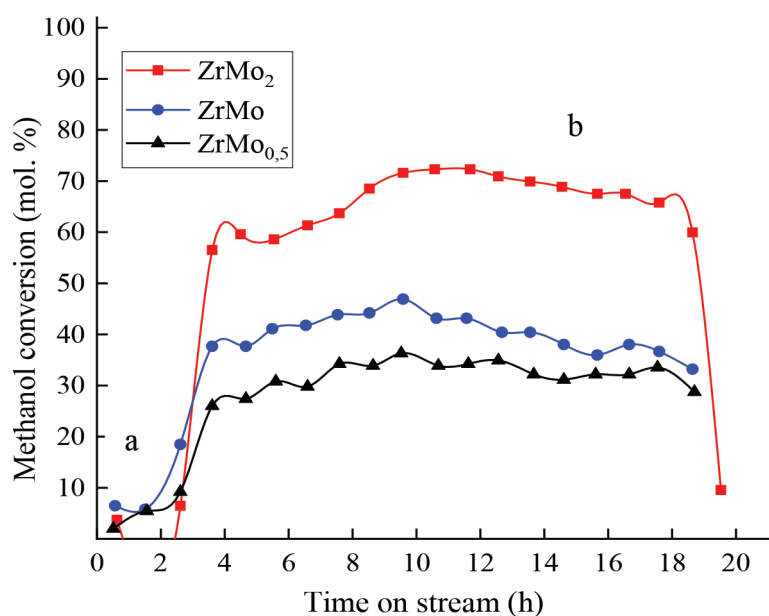


**Figure 3.** Variation of methanol conversion on catalysts Zr-Mo: a) after O<sub>2</sub>-treatment; b) after H<sub>2</sub>-treatment, reaction temperature – 473 K.

The nonstoichiometric composition of ZrMo<sub>2</sub> catalyst surface after O<sub>2</sub> + H<sub>2</sub>-treatment led to an increase in the activity of the sample at a reaction temperature of 473 K. Figure 5 shows that in the course of catalysis, the conversion of methanol increased from 56.5% to 72.6% due to the further formation of an active surface under conditions of aerobic oxidation of methanol.

Ability of the surface to absorb hydrogen with the formation of hydride phases plays an important role in formation of the active surface of alloys. While zirconium acts as a hydride-forming component in its alloys, vanadium acts as such a component in the VFe alloy. The ability of vanadium to form numerous compounds with both oxygen and hydrogen makes it unique. Figure 4 shows the change in the catalytic activity of the VFe<sub>0.2</sub> alloy after O<sub>2</sub>-treatment (T 873 K, 3 h)

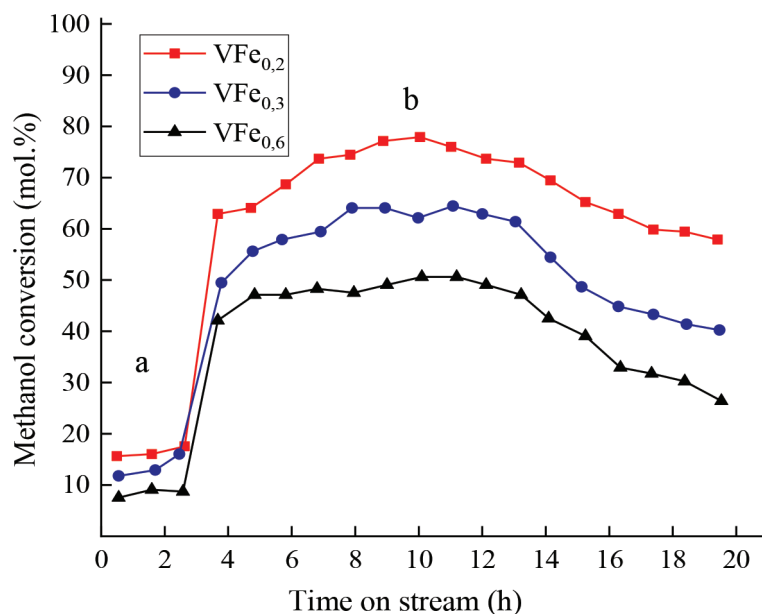


**Figure 4.** Variation of methanol conversion on catalysts V-Fe; a) after O<sub>2</sub>-treatment; b) after H<sub>2</sub>-treatment, reaction temperature – 473 K.

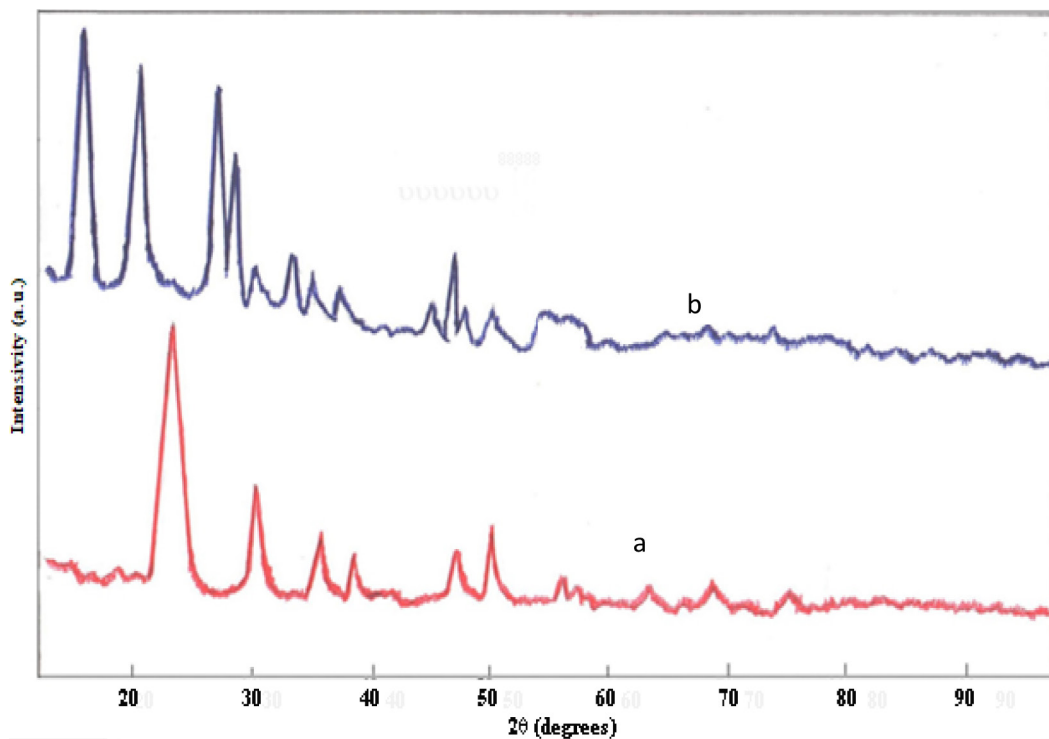


**Figure 5.** XRD patterns of catalyst based on an alloy ZrMo<sub>2</sub>; a) after O<sub>2</sub>-treatment, 873K, 3h, b) after H<sub>2</sub>-treatment, 873 K, 1 h.

and H<sub>2</sub>-treatment (T 873 K, 1 h). The observed phase changes on the contact surface are shown in Figure 6 (Supplemental Table 5).

On the surface of the initial VFe<sub>0.2</sub> alloy, as can be seen from Supplemental Table 5, mainly metal-vanadium (at 2θ = 41.3; 42.2; 62.6), and insignificantly - V<sub>2</sub>O<sub>3</sub> oxide (at 2θ = 32, 7; 35.1) are present. No iron phase was detected.

**Table 3.** Changes in the activity of  $ZrV_{0.3}ZrMo_2$  and  $VFe_{0.2}$  catalysts after  $O_2$ - and  $H_2$ -treatment.

№	Conditions	T, K	Reaction yield, mol, %					Selec. DMM mol.%	Conver. mol. %
			CO <sub>2</sub>	FA	DME	DMM	MF		
1.	Initial $ZrV_{0.3}$	673	27.3	-	-	-	-	-	27.3
2.	$ZrV_{0.3}$ Air, T 873 K, 3h	423	-	-	2.0	-	-	-	2.0
		473	-	9.6	-	-	-	-	9.6
		523	-	19.6	-	-	-	-	19.6
		573	1.1	45.2	-	-	-	-	46.2
		623	2.3	69.8	-	-	-	-	73.1
3.	$ZrV_{0.3}$ Air, T 873 K, 3h $H_2$ -, T 873 K, 1h	423	0.1	20.3	4.8	41.0	1.0	61.0	67.2
		473	0.8	22.6	11.5	38.0	2.4	50.4	75.3
		523	2.0	28.2	20.8	33.4	3.9	37.8	88.3
		573	3.0	25.7	38.0	28.6	6.7	28.6	100
		623	5.2	20.2	37.3	25.0	12.3	25.0	100
4	Initial $ZrMo_2$	673	20.5	-	-	-	-	-	20.5
5.	$ZrMo_2$ Air, T 873 K, 3h	423	-	weak	-	-	-	-	-
		473	-	6.0	-	-	-	-	6.0
		523	-	21.6	-	-	-	-	21.6
		573	0.7	42.2	-	-	-	-	42.2
		623	2.2	51.9	-	-	-	-	53.9
6.	$ZrMo_2$ Air, T 873 K, 3h $H_2$ -, T 873 K, 1h	423	0.1	18.1	5.1	39.3	0.8	62.0	63.4
		473	1.9	22.0	10.2	37.1	1.4	51.1	72.6
		523	2.2	27.0	21.3	32.7	3.1	37.9	86.3
		573	3.0	29.7	36.8	26.0	4.5	26.4	98.6
		623	5.1	25.0	38.3	24.2	7.4	24.2	100
7	Initial $VFe_{0.2}$	673	21.4	-	-	-	-	-	21.4
8	$VFe_{0.2}$ Air, T 873 K, 3h	423	-	-	-	-	-	-	14.7
		473	-	15.2	-	-	-	-	15.2
		523	-	22.9	-	-	-	-	22.9
		573	0.5	42.5	-	-	-	-	43.0
		623	2.3	55.0	-	-	-	-	57.3
9	$VFe_{0.2}$ Air, T 873 K, 3h $H_2$ -, T 873 K, 1h	423	-	21.0	3.5	43.1	1.1	62.7	68.7
		473	0.6	23.3	12.0	39.4	2.5	50.6	77.8
		523	1.8	27.5	25.2	31.9	4.8	35.0	91.2
		573	2.8	29.1	35.7	27.7	4.7	27.7	100
		623	6.0	24.2	39.0	23.1	7.7	23.1	100

As a result of oxidative treatment with air (T 873 K, 3 h), the formation orthorhombic and tetragonal oxide  $V_2O_5$  phase is observed on the catalyst surface (at  $2\theta = 20.6; 24.6; 27.0; 32.5; 50.2$ ; Figure 6). Formation of the  $VO_2$  phase ( $2\theta = 26.3; 37.1; 42.0; 56.5$  JCPDS: 43-1051), other  $VO_x$  oxides, mixed oxides, which are formed in large quantities by vanadium with oxygen, are possible as well. However, the activity of the  $VFe_{0.2}$  catalyst remains at a low level. Only after  $H_2$ -treatment (T 873 K, 1 h), drastic increase in the activity of the sample observed (Figure 4), which is obviously associated not only with a change in the phase composition of the surface, but also with the valence state of the components. If after  $O_2$ -treatment there was no iron phase on the sample surface, then after  $H_2$ -treatment there is a segregation of iron on the surface, its

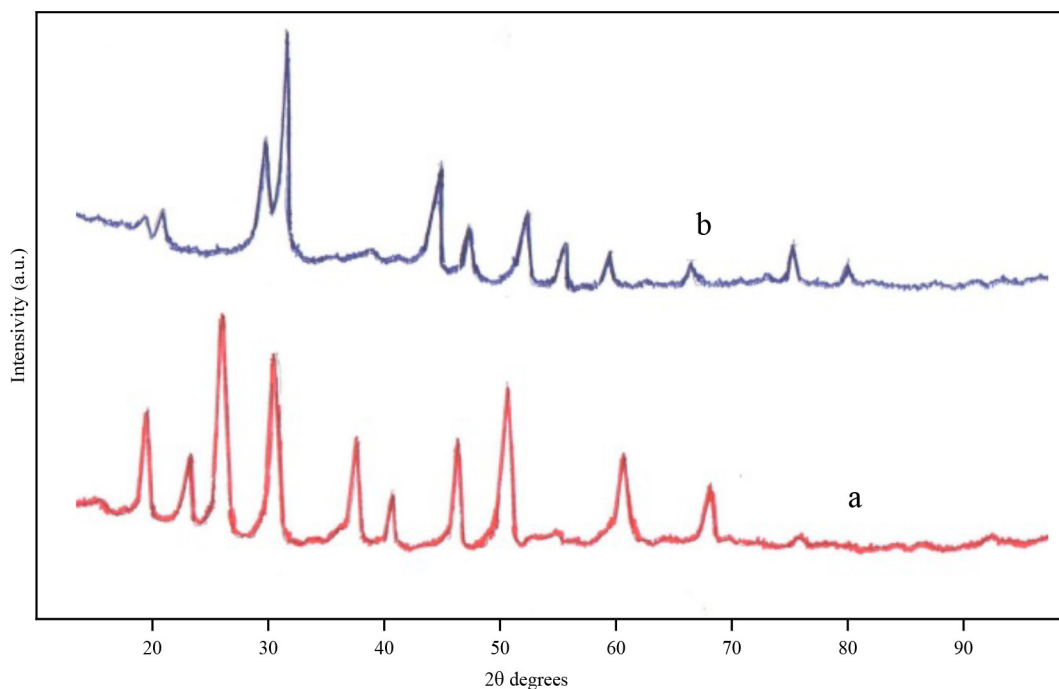


**Figure 6.** XRD patterns of catalyst based on an alloy  $VFe_{0.2}$ : a) after  $O_2$ -treatment, 873 K, 3 h; b) after  $H_2$ -treatment, 873 K, 1 h.

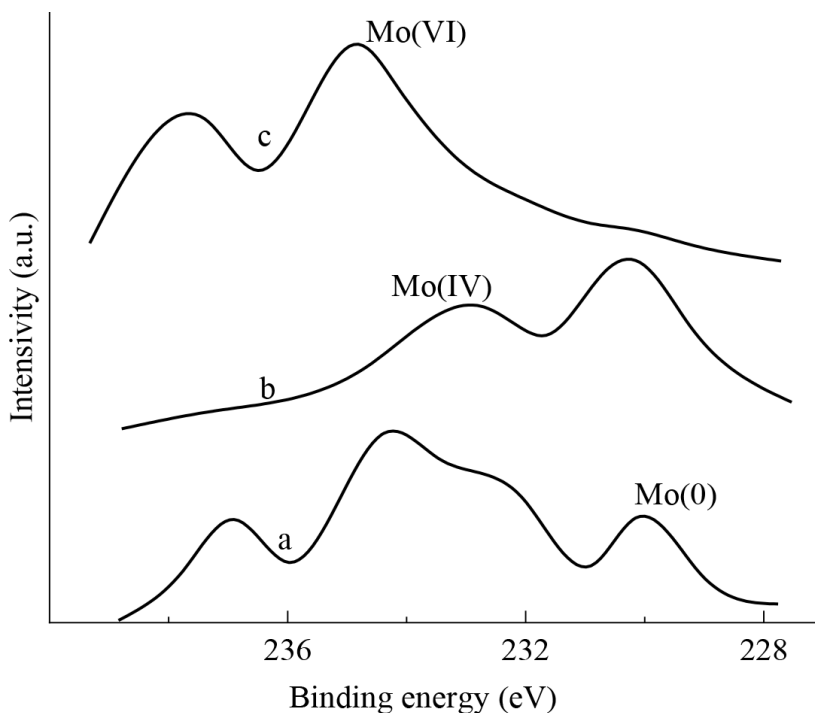


**Figure 7.** X-ray photoelectron spectra of catalyst  $ZrMo_2$ . a) Initial. b) After  $H_2$ -treatment, 873 K, 1 h. c) After  $O_2$ -treatment, 873K, 3 h.

oxidation, the appearance of new peaks of  $\alpha-Fe_2O_3$ , FeO mixed with  $Fe_3O_4$ , possibly mixed with vanadium Fe-V-O of various compositions, the phases which are almost impossible to establish.

According to thermodynamic data, iron (II), and vanadium (III, IV, V) oxides have close Gibbs energies ( $\Delta G_{298}^\circ (VO) = -402.6 \text{ kJ/mol}$ ;  $\Delta G_{VO_2} = -665.0$ ;  $\Delta G_{FeO} = -244.3$ ;  $\Delta G_{Fe_2O_3} = -740.3$ ;  $\Delta G_{V_2O_3} = -1139.4$ ;  $\Delta G_{V_2O_5} = -1421.2$ ), and the formation

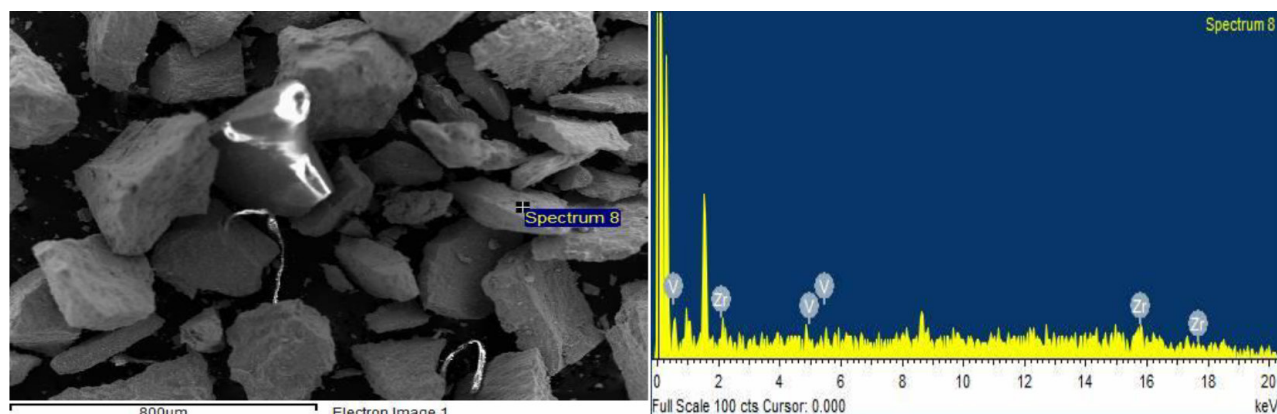


Figure 8. SEM image (a) and EDX spectrum (b) of  $ZrV_{0.3}$  catalyst after  $O_2$ -treatment (873 K, 3 h).

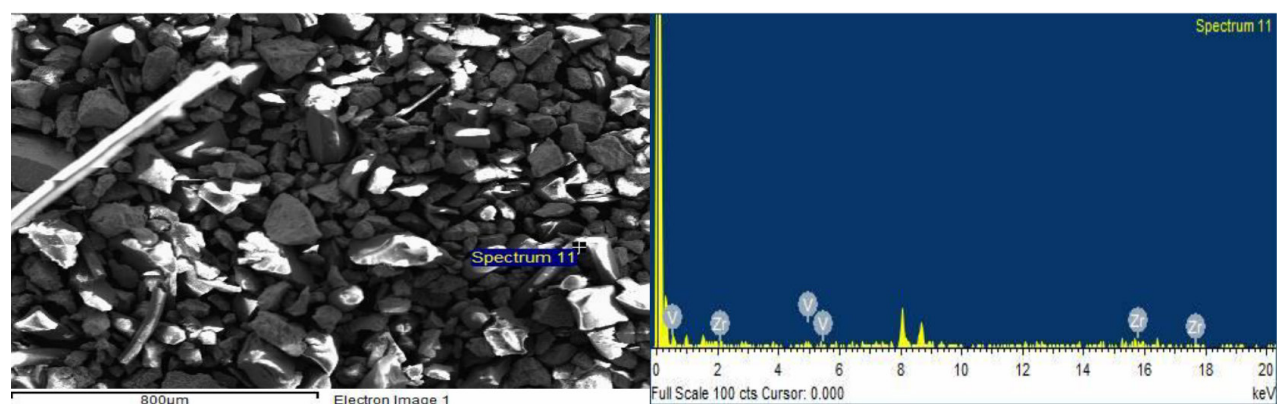


Figure 9. SEM image (a) and EDX spectrum (b) of  $ZrV_{0.3}$  catalyst after  $H_2$ -treatment (873 K, 1 h).

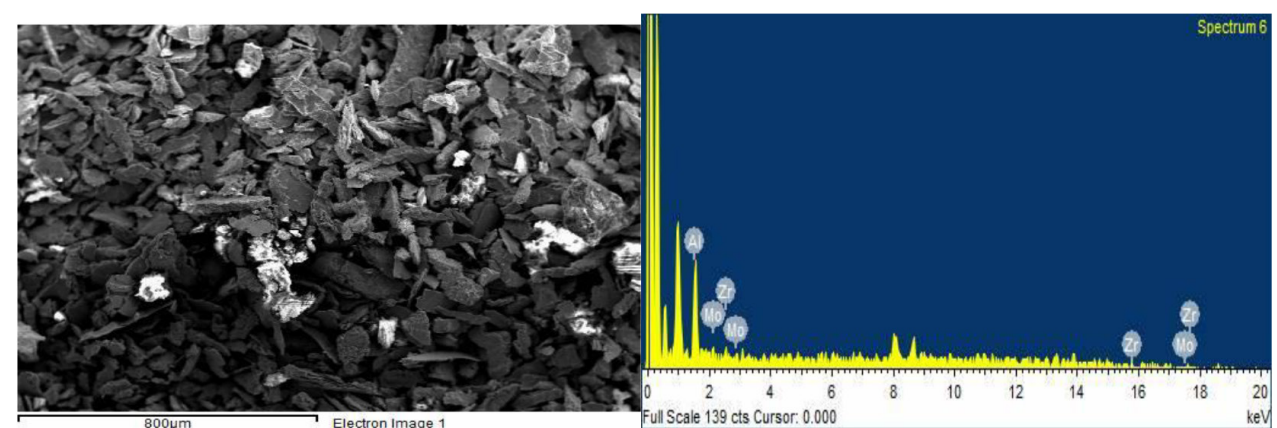


Figure 10. SEM image (a) and EDX spectrum (b) of  $ZrMo_2$  catalyst after  $O_2$ -treatment (T 873 K, 3 h).

of such oxides is not excluded. Formation of nonstoichiometric oxides  $V_4O_9$ ,  $V_3O_7$ ,  $V_2O_4$  of different structures after  $H_2$ -treatment is also possible. In homogeneous composition of the surface, as well as the presence of anionic vacancies, changes in the valence state of the components led to an increase in the activity of  $VFe_{0.2}$  after  $O_2 + H_2$ -treatment.

The analysis of the alloys surface and the state of the components of the alloys before and after the  $O_2$ - and  $H_2$ -treatment were carried out by X-ray photoelectron spectroscopy (XPS) method on a VIEE-15 and ADES-400 spectrometer. Figure 7 shows the X-ray spectra of the  $ZrMo_2$  intermetallic compound depending on the processing conditions.

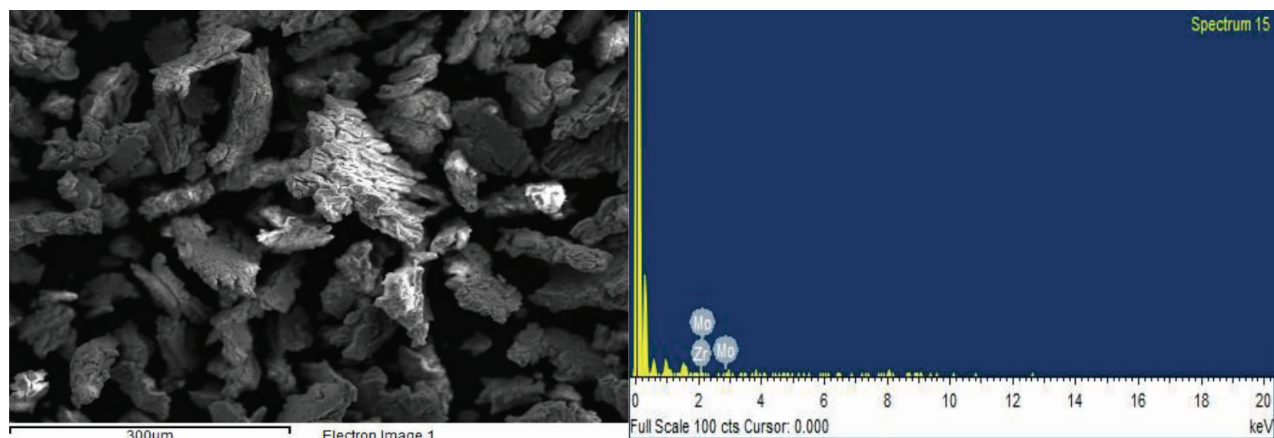


Figure 11. SEM image (a) and EDX spectrum (b) of  $ZrMo_2$  catalyst after  $H_2$ -treatment (T 873 K, 1 h).

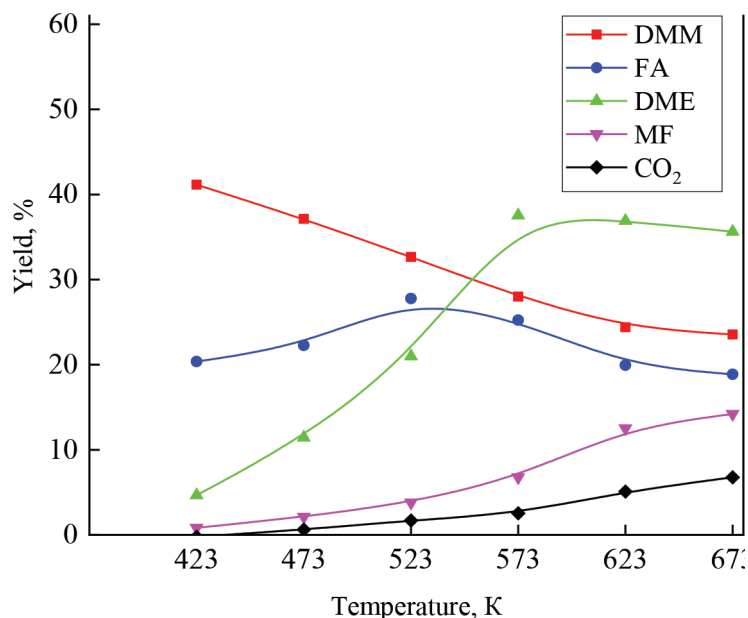
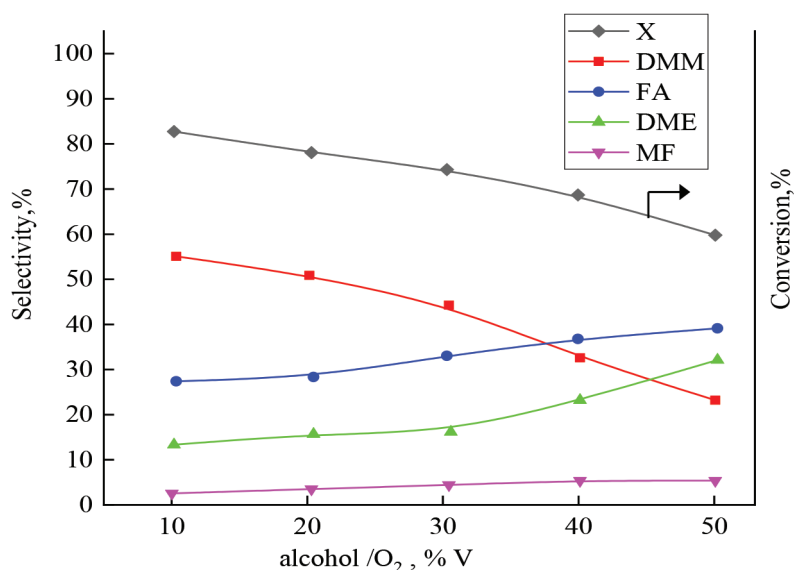


Figure 12. Variation of reaction yield with the reaction temperature on  $ZrV_{0.3}$  catalyst after  $O_2 + H_2$ -treatment.

On the initial surface of the sample, molybdenum is present in several valence states - in the form of an oxide, in the form of a compound in an intermediate oxidation state, and in a metallic state. Vacuum heat treatment of the sample surface by bombardment with  $Ar^+$  ions leads to an increase in the fraction of Mo in the zero-valent state. The binding energy of Mo  $3d_{5/2}$  in the zero-valence state is  $228.1 \pm 0.1$  eV. Oxidation treatment with air at T 873 K caused significant changes, mainly in the valence state of molybdenum. With an increase in the oxidation temperature, molybdenum completely transforms into a hexavalent state, the binding energy is  $234.2 \pm 0.1$  eV, and the Mo/Zr ratio in the surface layer increases by 1.4 times. The reduction of the oxidized sample with hydrogen (T 873 K, 1 h) leads to the appearance of Mo ions in the surface layer in an intermediate oxidation state: Mo (0); Mo (IV); Mo (VI) - Table 2.

The shape and position of the Mo  $3d$  signal undergoes the greatest changes depending on the processing conditions. In the  $ZrMo_2$  sample, it was possible to identify three oxidation states of molybdenum:  $Mo^{6+}$ ,  $Mo^{4+}$ , and  $Mo^0$ , which correspond to the binding energy of  $234.2 \pm 0.3$ ;  $230.3 \pm 0.2$  and  $228.0 \pm 0.2$  eV. As can be seen from Figure 3, the activity of the  $ZrMo_2$  catalyst after  $O_2$ -treatment increases insignificantly, although the presence of Zr ( $Mo_4$ )<sub>2</sub> and  $MoO_3$  phases, i.e.,  $Mo^{6+}$  ion, was established on the surface. However, after  $H_2$ -treatment, the activity of the test sample increases significantly.



**Figure 13.** Variation of the selectivity to FA, DME, DMM with alcohol/O<sub>2</sub> ratio on VFe<sub>0.2</sub> catalyst at T 473 K.

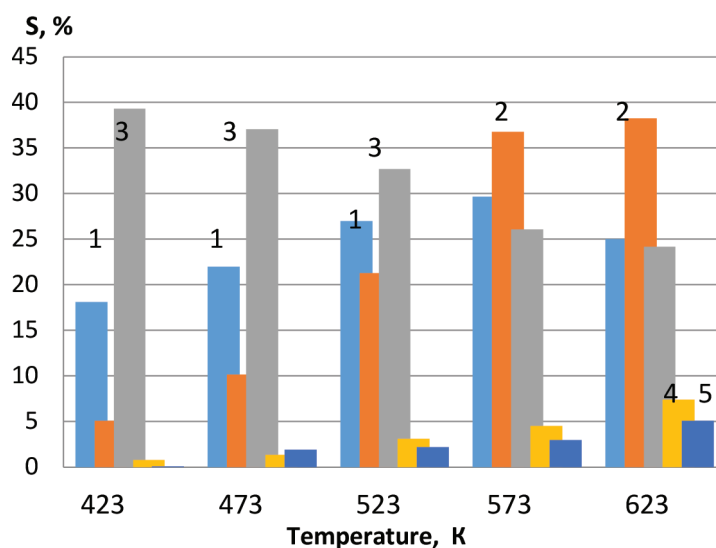


**Figure 14.** Diagram of the selectivity to FA, DME, DMM with the reaction temperature on ZrMo<sub>2</sub> catalyst; 1-FA, 2-DME, 3-DMM, 4-ME, 5-CO<sub>2</sub>.

According to XPS data, the presence of Mo<sup>4+</sup> and Mo<sup>0</sup> ions was detected on the surface, which is consistent with XRD analysis data. In the course of catalysis, under conditions of aerobic oxidation of methanol, the activity of the catalyst continues to increase due to the further formation of the active surface. The process continues until the optimum oxidation state of Mo is achieved. Such a catalyst worked in catalysis with high efficiency for more than 20 hours, after which there was a tendency for a gradual decrease in activity. Subsequent additional oxidation in a stream of air at T 873 K, 1 h. leads to a significant decrease in activity – Figure 3. This confirms the relationship between the oxidation state of molybdenum and the activity of the system. The optimal oxidation state of the catalyst in this process is obviously the presence of the Mo<sup>5+</sup> ion. The activity of the Mo<sup>5+</sup> ion in catalytic processes has been confirmed in a number of studies. Thus, in a study by C. Ranga et al. [30], an evaluation of the surface composition and state of Mo surface particles was carried out on samples of MoO<sub>3</sub>/ZrO<sub>2</sub> catalysts, fresh and reduced with H<sub>2</sub>/CH<sub>4</sub> (XPS). The fresh sample contained only Mo<sup>6+</sup> particles, and moderate reduction of the MoO<sub>3</sub> sample at T 623 K resulted in the presence of Mo<sup>5+</sup> particles along with Mo<sup>6+</sup>, as

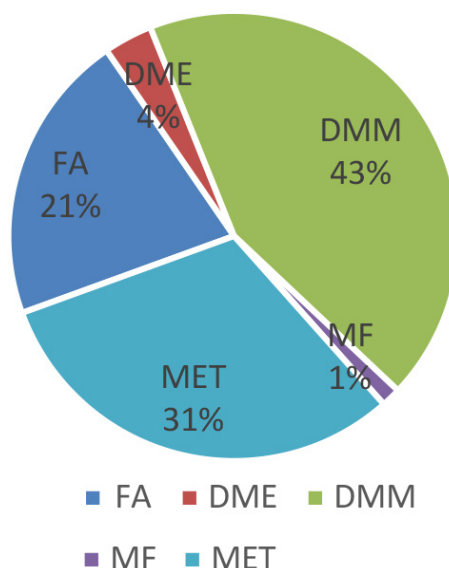


**Figure 15.** Diagram of distribution products of the methanol oxidation on  $VFe_{0.2}$  catalyst at T 423 K after  $O_2 + H_2$  treatment.

well as  $Mo^{4+}$ . The binding energies were calculated for  $Mo^{6+}$ ,  $Mo^{5+}$ ,  $Mo^{4+}$  (232.0–232.4, 231.0–231.6, and 229.1–229.7 eV, respectively). The presence of  $Mo^{5+}$  particles in reduced samples, according to the authors, indicated the creation of active defects in the structure of the starting oxide, which led to an increasing activity. It was also reported that  $Mo^{5+}$  particles appeared as a result of the reduction of  $MoO_3$  to  $MoO_{3-x}$ .

$O_2 + H_2$ -treatment led to changes not only in the composition of the surface layer, but also to changes in the valence state of the active components of the alloy - V, Mo, as evidenced by the results of XPS analyzes and another -  $VFe_{0.2}$  alloy catalyst. Formation of  $VOx$ ;  $VO_{2-x}$ ;  $V_2O_{3-x}$ ;  $V_2O_{5-x}$ ;  $V_3O_7$ ;  $V_4O_9$ ; Fe-Vx-Oy oxides and other compounds of nonstoichiometric composition on the sample surface after  $O_2 + H_2$  - treatment, the presence of anionic vacancies, the presence of defects – all contributed to the creation of active centers of two  $V^{4+}$  and  $V^{5+}$  ions on the catalyst surface (two peaks 2p 3/2 at 515.3 eV and 516.9 eV discovered by XPS belong to vanadium). The presence of an active  $V^{4+} \leftrightarrow V^{5+}$  site on the contact surface promoted an increase in the activity of  $VFe_{0.2}$  catalyst in the methanol oxidation reaction.

The surface of  $ZrV_{0.3}$  and  $ZrMo_2$  catalysts before and after  $O_2 + H_2$  - treatment was also investigated by the SEM method and is explained in Figures 8 (a, b), 9 (a, b) and Figures 10 (a, b), 11 (a, b).

As seen from the micrographs (SEM image), as a result of  $O_2$ - treatment, the segregation of catalyst active components (V, Mo) on the surface increases, and accordingly increases the activity. After  $H_2$ -treatment, according to EDX spectrum, the V/Zr ratio and Mo/Zr slightly decreases, however, the activity of the samples increases.

Previous researches have shown that the effectiveness of catalysts is determined mainly by the presence of active sites on its surface associated with the influence of acid-base sites, with synergistic effect, with the presence of charged particles such as  $Mo^{5+}$ . Our results confirm the influence of these factors, adding that the  $O_2$ - and  $H_2$ -treatment is an effective method for the formation of active centers on the surface, and under certain conditions can affect the yield and selectivity of the obtained oxidation products. In this case, alloys can be considered a model for studying the conditions for the formation of active centers on the surface of contacts.

### 3.2. Oxidative dehydrogenation of methanol

Oxidation-reduction treatment led to qualitative changes in the surface composition due to the segregation of the active components of alloys (Mo, V) of variable valence on the catalyst surface, and then to the implementation of the optimal degree of their oxidation under catalysis conditions. The increase in activity was associated with the appearance of Mo and V in these catalysts in an intermediate oxidation state.

The analysis of the catalytic activity of  $ZrV_{0.3}$ ,  $ZrMo_2$ , and  $VFe_{0.2}$  samples was carried out on a flow-through unit, corresponding diagram is given in the appendix (Supplemental Figure 1S). Weighed portions of catalysts in an amount of 0.3 g were crushed, mixed with crushed quartz in a ratio of 1:10, then, were loaded into a tubular quartz reactor. Following  $O_2$  and  $H_2$ -treatment, reactor was placed in gas thermostat, where a constant temperature was maintained. Analysis of

primary samples was performed (for a description, see Section 2.3). Alcohol was fed into the reaction using nitrogen in a bubbling manner through a saturator placed in a liquid thermostat at a rate of 1.5–1.8 L/h. With an increase in the thermostat temperature, the partial pressure of alcohol increased. Oxygen was also supplied to the reactor from the cylinder, after passing purification system (alcohol: O<sub>2</sub> ratio = 1 ÷ 5). GHSV - gas hourly space velocity in terms of the catalyst volume (V cat. ~ 1.5 cm<sup>3</sup>) was in the range of 0.5–1.2 h<sup>-1</sup>. After reaching the stationary mode, samples were obtained on a six-way valve, directly into the chromatograph. The volume of the exiting gas mixture was recorded on a gas meter at the outlet of the system. The reaction was performed at the temperature range 423–623 K. The most active samples were ZrV<sub>0.3</sub>, ZrMo<sub>2</sub> and VFe<sub>0.2</sub> after H<sub>2</sub>-treatment (T 873 K, 1 h) in the oxidative dehydrogenation of methanol at T 473 K. These include samples with a lower content of the active component, except for the ZrMo<sub>2</sub> intermetallic compound.

The impact of temperature on the methanol oxidation reaction final products yield on the ZrV<sub>0.3</sub> catalyst is shown in Figure 12. With an increase in the reaction temperature, the yield of DMM – decreases, but the yield of DME increases; meanwhile, the yield of FA passes through a maximum in the temperature range 423–473 K. When decreasing the temperature to 423 K, the DMM yield increases. A similar picture is observed for other catalysts, such as ZrMo<sub>2</sub>; VFe<sub>0.2</sub> - Table 3.

For the quantitative determination of the obtained reaction products, the internal standard method was used, taking into consideration the correction factors, which were determined as the tangent of the straight line's slope [33]. The values of conversion, selectivity and yields of reaction products were calculated according to the following formulas, which are presented in appendix (see Supplementary Material).

Figure 13 shows the correlation of selectivity (to FA, DMM, DME, MF), with initial concentration of alcohol (i.e., on the ratio of alcohol/O<sub>2</sub>) at T 473K.

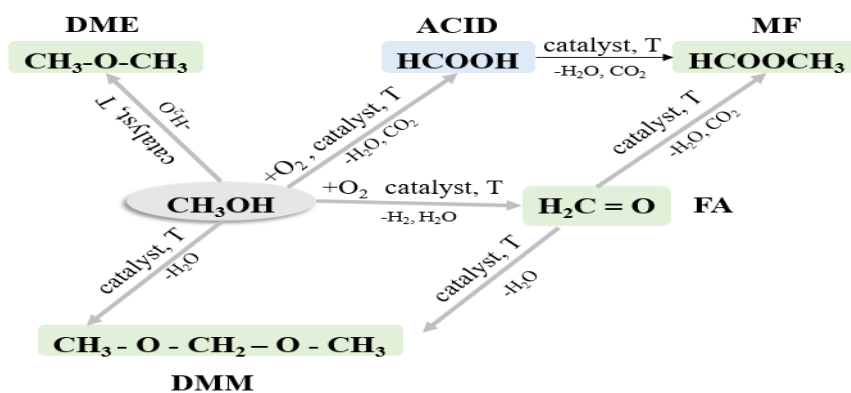
At a ratio of alcohol/O<sub>2</sub> of 1/3, the conversion of methanol on the VFe<sub>0.2</sub> catalyst after O<sub>2</sub> + H<sub>2</sub>-treatment was 77.8%, the selectivity for FA = 29.9%; DMM = 50.6%; DME = 15.4%, MF = 3.4%. With an increase in the alcohol: O<sub>2</sub> ratio, the conversion of methanol and the selectivity for DMM at this temperature decreases, however, the selectivity for FA and DME slightly increases. A diagram at Figure 14 shows correlation of the selectivity of methanol oxidation products on ZrMo<sub>2</sub> catalyst with the reaction temperature.

As seen from the Figure 14, with an increase in temperature, the selectivity for DMM decreases, while selectivity for DME, MF, and CO<sub>2</sub> increases. The highest yield of DMM with a methanol conversion of 68.7% was observed on another catalyst - VFe<sub>0.2</sub> after O<sub>2</sub> + H<sub>2</sub>-treatment at a reaction temperature of 423 K (43%). Diagram at Figure 15 shows distribution of methanol oxidation products. According to the catalytic results, a reaction Scheme can be proposed (see Scheme 1).

Compared to the catalyst samples oxidized in a stream of air, the hydrogenated samples of the ZrV0.3; ZrMo2 and VFe0.2 alloys showed higher activity and selectivity for formaldehyde. As a result of the “soft” reductive H<sub>2</sub> treatment of the catalysts (T 873 K, 1 h), a decrease in the temperature threshold of the onset of the reaction by ~ 100–150 K was observed, which is associated with the activity of the hydride subsystem at the temperature range of T 473–523 K, which is explained in Table 3.

#### 4. Conclusion

It is proved that bimetallic catalysts based on Zr alloys with V, Mo, Fe show rather high activity and selectivity in the reaction of methanol oxidation to FA, DME, and DMM after O<sub>2</sub> + H<sub>2</sub>-treatment. This happens due to the segregation of



**Scheme:** According to the catalytic results, a reaction Scheme can be proposed

the active components of alloys (V, Mo) on the surface of the catalysts in an intermediate oxidation state and, further, to the realization of their optimal oxidation state under catalysis conditions. This is evidenced by the results of XRD, XPS, and SEM analyzes.

It is assumed that the presence of  $V^{4+} \leftrightarrow V^{5+}$  and  $Mo^{4+} \leftrightarrow Mo^{5+} \leftrightarrow Mo^{6+}$  ions and the related effect of the “electronic factor” in catalysis is enhanced in the presence of hydrogen “in situ”. It is also shown that the presence of the hydride subsystem shifts the temperature threshold of the onset of the  $CH_3OH$  oxidation reaction towards a decrease in the reaction temperature by  $\sim 100$ – $150$  K. The nonstoichiometric composition of the surface layer of catalysts after  $O_2 + H_2$ -treatment, the presence of anionic vacancies, the presence of a hydride subsystem, apparently, facilitated electronic transitions in bimetallic systems of Zr – V, Zr – Mo, V-Fe -catalysts. For d-elements, which included Zr, V, Mo metals, such electronic transitions were not associated with high-energy costs, and the presence of hydrogen “in situ” in these systems enhanced the influence of the “electronic factor”. The influence of these factors caused an increase in the activity of bimetallic catalysts based on Zr-V, Zr-Mo and V-Fe alloys.

## References

1. Nierhoff A, Conradsen C, McCarthy D, Johansson TP, Chorkendoff I. Adsorbate induced surface alloy formation investigated by near ambient pressure X-ray photoelectron spectroscopy. *Catalysis Today: Heterogeneous Catalysis and Surface Science* 2015; 244: 130-135. doi: 10.1016/j.cattod.2014.06.024
2. Vedyagin AA, Shubin YV, Volodin AM, Stoyanovskii VO, Kenzhin RM et al. Stabilization of active sites in alloyed Pd-Rh catalysts on  $Al_2O_3$  support. *Catalysis Today* 2014; 238: 80-86. doi: 10.1016/j.cattod.2014.02.056
3. Brailovsky SM., Temkin ON, Trofimov IV. Oxidation of alcohols on metals of the copper subgroup. *Problems of kinetics and catalysis. Digest of Articles, Moscow, “Science”* 1985; 19: 146-175. (in Russian)
4. Millar G, Collins M. Industrial production of formaldehyde using polycrystalline Ag- catalyst. *Industrial & Engineering Chemistry Research* 2017; 56 (33): 9247-9265. doi: 10.1021/acs.iecr.7b02388
5. Zhukov AB, Rumyantsev RN, Ilyin AA, Ilyin AP. Oxidation of methanol to formaldehyde at industrial conditions using various Fe-Mo-catalysts. *Chemistry and Chemical Technology* 2016; 59 (5): 65-71. (in Russian)
6. Sun J, Yang G, Yoneyama Y, Tsubaki N. Catalysis chemistry of DME synthesis. *ACS Catalysis* 2014; 4 (10): 3346-3356. doi: 10.1021/cs500967j
7. Bateny H, Able C. Development of heterogeneous catalysts for the dehydration of methanol to DME. *Catalysis in Industry* 2018; 10 (4): 6-30. (in Russian)
8. Nikonova OA, Capron M, Fang G, Faye J, Gulaim A. et.al. Novel approach rhenium oxide catalysts for selective oxidation to DMM. *Journal of Catalysis* 2011; 279 (2): 310-318. doi: 10.1016/j.jcat.2011.01.028
9. Faye J, Capron M, Takahashi A, Paul S, Katrynoik B, et.al. Effect of oxomolybdate species dispersion on direct methanol oxidation to dimethoxymethane over  $MoOx/TiO_2$  catalysts. *Energy Science & Engineering* 2015; 3 (2): 115-125. doi: 10.1002/ese3.53
10. Chen S, Ma X. The role of oxygen species in the selective oxidation of methanol to dimethoxymethane over  $VO_x/TS-1$  catalyst. *Journal of Industrial and Engineering Chemistry* 2017; 45: 296-300. doi: 10.1016/j.jiec.2016.09.037
11. Meng Y, Wang T, Chen S, Zhao Y, Ma X et al. Selective oxidation of methanol to DMM on  $V_2O_5-MoO_3/\gamma-Al_2O_3$  catalysts. *Applied Catalysis B: Environmental* 2014; (160): 161-172. doi: 10.1016/j.apcatb.2014.05.008
12. Zhao H, Bennici S, Shen J, Auroux A. Nature of surface sites of  $V_2O_5-TiO_2/SO_4^{2-}$  catalysts and reactivity in selective oxidation of methanol to DMM. *Journal of Catalysis* 2010; 272 (1): 176-189. doi: 10.1016/j.jcat.2010.02.028
13. Wang G, Xu H, Lu K, Ding Z et.al. One-pot synthesis of  $VOx/Al_2O_3$  as efficient catalysts for propane dehydrogenation. *Turkish Journal of Chemistry* 2020; 44 (1): 112-124. doi: 10.3906/kim-1907-53
14. Ellert OG, Tsodikov MV, Nikolaev SA, Novotortsev MV. Bimetallic nanoalloys in heterogeneous catalysis of industrially important reactions - synergism and structural organization of active components. *Russian Chemical Reviews* 2014; 83 (8): 718-732.
15. Forzatti P, Tronconi E, Elmi AS, Busca G. Methanol oxidation over vanadia-based catalysts. *Applied Catalysis A General* 1997; 157: 387-408. doi: 10.1016/S0926-860X(97)00026-4
16. Al-Ghamdi SA, De Lasa H. Propylene production via propane oxidative dehydrogenation over  $VOx/\gamma-Al_2O_3$  catalyst. *Fuel* 2014; 128: 120-140. doi: 10.1016/S0926-860X(97)00026-4
17. Tatibouet JM. Methanol oxidation as a catalytic surface probe. *Applied Catalysis A General* 1997; 148: 213-252. doi: 10.1016/S0926-860X(96)00236-0

18. Olthof B, Khodakov A, Bell AT, Iglesia E. Effects of support composition and pretreatment conditions on the structure of vanadia dispersed on  $\text{SiO}_2$ ,  $\text{Al}_2\text{O}_3$ ,  $\text{TiO}_2$ ,  $\text{ZrO}_2$  and  $\text{HfO}_2$ . *Journal of Physical Chemistry B* 2000; 104: 1516-1528. doi: 10.1021/jp9921248
19. Chen S, Ma F, Xu A, Wang L, Chen F, Lu W. Study on the structure, acidic properties of V-Zr nanocrystal catalysts in the oxidative dehydrogenation of propane. *Applied Surface Science* 2014; 289: 316-325. doi: 10.1016/j.apsusc.2013.10.158
20. Solsona B, Dejoz A, Garcia T, Concepción P, Lopez Nieto JM et al. Molybdenum-vanadium supported on mesoporous alumina catalysts for the oxidative dehydrogenation of ethane. *Catalysis Today* 2006; 117: 228-233. doi: 10.1016/j.cattod.2006.05.025
21. Lin X, Hoel CA, Sachtler WMH, Poepplmeier KR, Weitz E. Oxidative dehydrogenation (ODH) of ethane with  $\text{O}_2$  as oxidant on selected transition metal-loaded zeolites. *Journal of Catalysis* 2009; 265: 54-62. doi: 10.1016/j.jcat.2009.04.007
22. Blasco T, López Nieto JM. Oxidative dehydrogenation of short chain alkanes on supported vanadium oxide catalysts. *Applied Catalysis A: General* 1997; 157 (1-2): 117-142. doi: 10.1016/S0926-860X(97)00029-X
23. Wachs IE, Chen Y, Jehng JM, Briand LE, Tanaka T. Molecular structure and reactivity of the group V metal oxides. *Catalysis Today* 2003; 78: 13-24. doi: 10.1016/S0920-5861(02)00337-1
24. Shah PR, Baldychev I, Vohs JM, Gorte RJ. Comparison of redox isotherms for Vanadia supported on zirconia and titania. *Applied Catalysis A* 2009; 361: 13-17. doi: 10.1016/j.apcata.2009.03.036
25. Baldychev I, Gorte RJ, Vohs JM. The impact of redox properties on the reactivity of  $\text{V}_2\text{O}_5/\text{Al}_2\text{O}_3$  catalysts. *Journal of Catalysis* 2010; 269: 397-403. doi: 10.1016/j.jcat.2009.11.022
26. Hess, C. Nanostructured vanadium oxide model catalysts for selective oxidation reactions. *ChemPhysChem* 2009; 10: 319-326. doi: 10.1002/cphc.200800585
27. Haber J, Witko M, Tokarz R. Vanadium pentoxide I. Structures and properties. *Applied Catalysis A: General* 1997; 157 (1-2): 3-22. doi: 10.1016/S0926-860X(97)00017-3
28. Israei E, Wachs B, Weckhuysen M. Structure and reactivity of surface vanadium oxide species on oxide supports. *Applied Catalysis A: General* 1997; 157 (1-2): 67-90. doi: 10.1016/S0926-860X(97)00021-5
29. Komandur VR, Kondakindi C, Reddy R, Kishan J, Niemantsverdriet W et al. Structure and catalytic properties of molybdenum oxide catalysts supported on zirconia *Journal of Catalysis* 2004; 226 (1): 283-291. doi: 10.1016/j.jcat.2004.04.028
30. Ranga C, Lodeng R, Alexiadis VI, Rajkhova T, Detavernier C et al. Effect of composition and preparation of supported  $\text{MoO}_3$  catalysts for anisole hydride oxygenation. *Chemical Engineering Journal* 2018; 335 (1): 120-132. doi: 10.1016/j.cej.2017.10.090
31. Meng Y, Wang T, Shuang C, Zhao Y, Ma X et al. Selective oxidation of methanol to dimethoxymethane on  $\text{V}_2\text{O}_5$ - $\text{MoO}_3/\gamma$ - $\text{Al}_2\text{O}_3$  catalysts *Applied Catalysis B: Environmental* 2014, 160-161: 161-172. doi: 10.1016/j.apcatb.2014.05.008
32. Efendi AG, Magerramova LG, Aliyeva AM, Kojarova LI, Melikova IH. Catalysis for selective oxidation of methanol to formaldehyde and dimethoxymethane. *Science Technical Journal, Scientific Works* 2018; 4: 122-127 (in Azerbaijani).
33. Alieva AM, Efendi AJ, Magerramova LG, Babayev EM, Kozharova LI et al. Ways of production alternative kinds of fuels on the basis of methanol. *Oil Refining and Petrochemistry* 2019; 2: 27-32 (In Russian).

## Supplementary material

**Figure 1S.** Scheme of a flow-through installation.

1—vent scrubbing system, 2 — flow meter, 3 — traps, 4 — saturator, 5 — mixer, 6 — reactor, 7 — six-way valve, 8 — two - way valve, 9 — three - way valve, 10 — thermostat, 11 — heating furnace, 12 — condenser.

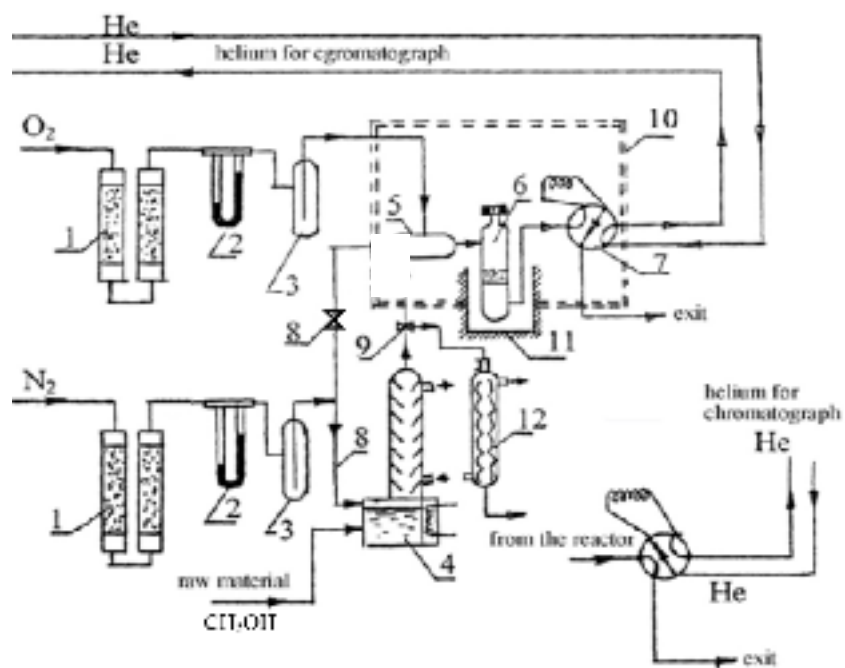


**Table 1.** XRD analysis outcomes for the initial  $ZrV_{0.3}$ .

№	Experimental data						Reference data						Filling cabinet
	$2\theta$	$d, \text{Å}$	I (a.u)	h	K	l	$2\theta$	$d, \text{Å}$	I (a.u)	h	k	l	JCPDS
1	32.026	2.792	100	1	0	0	31.60	2.960	100	1	1	1	
2	35.682	2.514	29.5	0	0	2	35.31	2.540	25	2	0	0	
3	37.762	2.380	15.4	1	0	0	50.15	1.830	65	2	0	2	37-1484
4	40.092	2.247	12.9	2	1	1	55.42	1.810	35	2	2	0	m- $ZrO_2$
5	51.592	1.770	12.5	1	0	2	60.35	1.547	45	3	1	1	
6	54.952	1.670	18.8	1	1	0	62.82	1.493	12	2	2	2	
7	62.260	1.490	29.4	1	0	3							
8	67.552	1.386	20.6	-	-	-	30.16	2.930	100	1	1	1	
							35.19	2.550	25	2	0	0	27-997
							50.65	1.801	50	2	0	2	t- $ZrO_2$
							60.34	1.534	20	3	1	1	
							68.82	1.471	5	2	2	2	

**Table 2.** XRD analysis outcomes for  $ZrV_{0.3}$  after  $O_2$ - and  $H_2$ -treatment.

№	Experimental data						Filling cabinet
	$2\theta$	$d, \text{Å}$	I (a.u)	H	K	L	JCPDS
<b>ZrV<sub>0.3</sub> after O<sub>2</sub>-treatment</b>							
1	20.010	4.433	13.8	1	0	1	41- 1426
2	22.410	3.964	14.5	1	1	0	o -V <sub>2</sub> O <sub>5</sub>
3	23.764	3.741	20.0	1	0	2	
4	24.615	3.614	8.9	0	1	1	
5	27.968	3.187	100	1	1	1	79-1976
6	31.171	2.867	47.6	1	1	1	t-V <sub>2</sub> O <sub>5</sub>
7	32.155	2.782	44.3	1	0	0	
8	33.683	2.659	24.9	0	0	2	
9	35.105	2.554	7.5	2	0	0	34-0187
10	40.514	2.225	18.8	2	1	1	V <sub>2</sub> O <sub>3</sub>
11	44.702	2.026	12.5	2	0	2	
12	50.106	1.819	46.1	2	2	0	
13	54.142	1.692	9.4	2	0	2	
14	55.064	1.667	23.5	0	1	3	
15	62.440	1.486	17.6	2	1	3	
<b>ZrV<sub>0.3</sub> after H<sub>2</sub>-treatment</b>							
16	21.2	2.723	11	1	1	0	
17	31.0	2.870	27.9	0	1	1	43-1051
18	32,4	2.795	100	1	0	1	VO <sub>2</sub>
19	35.3	2.546	38.9	0	0	2	
20	41.5	2.178	73.7	2	0	1	34-0187
21	42.3	2.133	26.1	2	0	0	V <sub>2</sub> O <sub>3</sub>
22	44.9	2.011	19.3	2	0	2	

**Table 3.** XRD analysis outcomes for the ZrMo<sub>2</sub> after O<sub>2</sub>-treatment.

№	Experimental data						Reference data						Filling cabinet
	2θ	d, Å	I (a.u)	h	k	l	2θ	d, Å	I (a.u)	h	k	L	JCPDS
Initial ZrMo <sub>2</sub>													
1	32.042	2.793	100	1	0	0	31.61	2.96	100	1	1	1	
2	35.821	2.511	29.7	0	0	2	35.31	2.54	25	2	0	0	37-1484
3	37.753	2.383	15.4	1	0	0	50.15	1.83	65	2	0	2	m-ZrO <sub>2</sub>
4	40.081	2.249	12.9	2	1	1	55.42	1.81	35	2	2	0	
5	49.560	1.839	12.5	1	0	2	60.35	1.55	46	3	1	2	
6	54.952	1.671	18.6	1	1	0							
7	62.255	1.491	28,7	1	0	3	30.16	2.93	100	1	1	1	27- 997
8	68.105	1.377	21.0				35.19	2.55	25	2	0	0	t- ZrO
							50.65	1.80	50	2	0	2	
							60.34	1.53	20	3	1	1	
ZrMo <sub>2</sub> after O <sub>2</sub> -treatment													
9	15.132	5.850	2	0	0	2	-	-	-	-	-	-	
10	23.180	3.834	100	1	1	2	23.13	3.84	100	1	1	2	21-1496
11	30.526	2.926	41	3	0	0	30.47	2.93	47	3	0	0	Zr(MoO <sub>4</sub> )
12	35.379	2.535	19	2	2	0	50.06	1.82	31	4	1	2	
13	38.661	2.327	10	2	2	2	-	-	-	-	-	-	
14	47.389	1.917	14	4	1	0	23.3	3.81	40	1	1	0	
15	50.033	1.822	23	1	1	6	25.9	3.44	100	0	4	0	76-1003
16	56.652	1.624	9	3	3	2	27.8	3.21	18	0	1	1	MoO <sub>3</sub>
17	57.494	1.602	8	5	0	3	33.3	2.69	11	0	2	1	
18	63.501	1.463	8	6	0	0	39.1	2.28	18	1	3	1	

**Table 4.** XRD analysis outcomes for the ZrMo<sub>2</sub> after H<sub>2</sub>-treatment.

№	Experimental data						Filling cabinet
	2θ	d, Å	I (a.u)	H	k	l	JCPDS
1	15.646	5.725	100	2	0	0	
2	21.034	4.220	87	2	0	2	H <sub>6</sub> Mo <sub>2</sub> O <sub>11</sub> Zr
3	24.565	3.621	71.3	3	1	0	
4	28.471	3.132	84	3	1	2	13-142
5	28.563	3.125	57	0	0	4	i-Mo <sub>4</sub> O <sub>11</sub>
6	34.437	2.602	24	4	0	2	
7	36.230	2.477	18.2	3	3	2	12-753
8	38.022	2.365	11.8	4	2	2	Mo <sub>9</sub> O <sub>26</sub>
9	47.612	1.908	27.3	6	0	0	
10	48.561	1.873	14.3	5	3	2	
11	50.533	1.805	15.8	3	1	6	01-1208
12	56.465	1.628	17.2	6	0	4	Mo (met)
13	68.648	1.366	50.0	5	2	7	
14	76.904	1.238	71.0	9	1	2	
15	79.203	1.208	42.0	6	0	8	

**Table 5.** XRD analysis outcomes for VFe<sub>0.2</sub> after O<sub>2</sub>- and H<sub>2</sub>-treatment.

№	Experimental data						Reference data			Filling cabinet
	2θ	d, Å	I (a.u)	H	k	L	2θ	d, Å	I (a.u)	JCPDS
Initial VFe <sub>0.2</sub>										
1	35.1	2.550	48	1	1	1	23.6	3.775	30	
2	41.3	2.181	100	1	1	0	32.7	2.730	100	34-0187
3	42.2	2.139	18.8	2	1	2	37.6	2.391	80	V <sub>2</sub> O <sub>3</sub>
4	44.7	2.026	37	0	1	2	41.8	2.157	20	
5	62.6	1.484	10	2	0	2	53.9	1.700	90	
VFe <sub>0.2</sub> after O <sub>2</sub> -treatment										
1	20.6	4.302	37	0	0	1	30.0	1.194	100	79-1976
2	24.6	3.615	32	0	1	1	50.7	1.799	80	t- V <sub>2</sub> O <sub>5</sub>
3	27.0	3.305	100	1	1	0	61.0	1.516	35	
4	32.5	2.751	85	0	3	1				
5	37.4	2.398	50	1	2	1	20.3	4.375	90	
6	41.4	2.175	20	1	3	0	26,6	3.348	100	41-1426
7	47.0	1.935	48	1	4	1	31.2	2.862	70	o-V <sub>2</sub> O <sub>5</sub>
8	50.2	1.816	70	2	2	0	34.3	2.610	50	
9	61.5	1.504	40	1	0	4	47.3	1.920	20	
10	67.2	1.392	25	1	1	3				
VFe <sub>0.2</sub> after H <sub>2</sub> -treatment										
1	21.0	4.226	5	-	-	-	26.3	3.371	100	
2	22.0	2.056	10	-	-	-	37.1	2.421	60	43-1051
3	31.0	2.882	31.7	-	-	-	42.0	2.150	15	VO <sub>2</sub>
4	32.0	2.794	100	-	-	-	56.5	1.628	50	
5	44.5	2.029	46.1	-	-	-				
6	48.0	1.893	20.9	-	-	-	33.3	2.69	100	24-0072
7	52.5	1.738	39.1	-	-	-	35.7	2.51	80	α-Fe <sub>2</sub> O <sub>3</sub>
8	54.6	1.679	15.2	-	-	-	54.1	1.69	51	
9	59.0	1.564	10.9	-	-	-	64.1	1.45	40	

10	67.5	1.384	7	-	-	-				
11	74.5	1.271	10.4	-	-	-	36.8	2.44	100	19-629
12	79.0	1.211	8.7	-	-	-	59.2	1.56	40	Fe <sub>3</sub> O <sub>4</sub>
							65.2	1.43	50	

## Definition of conversion, selectivity, yield

For the quantitative determination of the obtained reaction products, the internal standard method was used, taking into consideration the correction factors, which were determined as the tangent of the straight line's slope [33]:

$$S_i / S_{st} = f(g_i / g_{st}),$$

where  $S_i$ ,  $S_{st}$  - indicate areas of peaks of the analyte and the standard  $g_i$ ,  $g_{st}$  - are their weight ratios. Isopropanol was adopted as the standard.

The percentage of each component was calculated using the formula:

$$C_i = \frac{S_i k_i}{\sum S_i k_i} \cdot 100\%,$$

$k_i$  - correction factors for the reaction components.

The values of conversion, selectivity and yield presented in Table 8, were calculated according to the following formulas:

$$\text{Conversion of CH}_3\text{OH: } X, \% = \frac{C_{al}^0 - C_{al}^{res}}{C_{al}^0},$$

$C_{al}^{res}$  - alcohol residue

$$\text{Selectivity of i - product: } S_i, \% = \frac{C_i}{\sum C_i},$$

Yield of i- product:  $W_i, \% = X \times S_i$ .